Astron. Astrophys. 326, 831–841 (1997)

ASTRONOMY
AND
ASTROPHYSICS

Dust scattering and kinematics within the envelope of IRAS 09371+1212

J.P. Phillips[1] **and L. Cuesta**[2]

[1] Instituto Nacional de Astrofisica, Optica y Electronica, A. Postal 51 y 216 Pue., Puebla, Mexico
[2] Instituto de Astrofisica de Canarias, La Laguna, Tenerife, Spain

Received 24 April 1996 / Accepted 18 February 1997

Abstract. We have acquired narrow and broad band imaging, together with high and low resolution spectroscopy for the source IRAS 09371+1212. As a result, we are able to show the presence of systematic colour gradients within the interior and exterior envelopes. Whilst the interior bright lobes are characterised by relatively high values of $V-R$ (a regime of reddening which also extends asymmetrically to the east), the exterior shell possesses an annulus of lower $V-R$; an index which gradually increases again to larger radii. Such trends are, in part, characteristic of reflection nebulae, and may also indicate an evolution in grain properties with radial displacement from the nucleus; although gradients $V-R/B-V$ appear inconsistent with either normal interstellar dust or model ice grains.

Spectroscopy of a narrow $H\alpha$ absorption feature has further been used to evaluate the variation of grain scatter velocity along the source major axis. The results are inconsistent with previous measures in indicating a substantially invariant velocity for the southerly lobe, and a trend towards systematically increasing velocities in the northern lobe; there is no evidence to favour appreciable velocity decrements. In addition, we note evidence for strongly variable line width and depth. These may be explained in terms of a non-spherically symmetric scatter model providing grain sizes are modest, lobe densities are broadly invariant, and there are appreciable levels of both shell extinction and multiple and forward grain scattering. Alternative explanations in terms of cavity outflow models are also discussed.

Finally, we note that the presumed post-main-sequence status of this source is not necessarily inconsistent with a high galactic latitude, and that the height of the source above the galactic plane may be less than supposed from its observed luminosity.

Key words: dust extinction – jets and outflows – kinematics and dynamics – reflection nebulae – planetary nebulae: Frosty Leo

Send offprint requests to: J.P. Phillips

1. Introduction

IRAS 09371+1212 ("Frosty Leo") is an unusual bipolar outflow source with exterior ansae located some 12 arcsec from the nucleus. The nebula was first discovered by Forveille et al. (1987) as part of a survey of IRAS sources having unusual colour indices, and found to possess a strong, well defined CO emission profile with width $49\,\mathrm{km\,s^{-1}}$. Both the morphology of the source, and nature of the molecular emission appeared consistent with identification as a galactic outflow envelope; although the strongly peaked FIR continuum seems in that case to be anomalous, and suggestive of appreciable band emission by ice.

The nebula has subsequently been the subject of numerous investigations, from which it appears that the primary illuminating star has spectral type M4 (I?) $\Rightarrow$ K7 (II$\Rightarrow$III) (Forveille et al. 1987, Mauron et al. 1989), and forms part of a binary system with orientation orthogonal to the nebular major axis (Roddier et al. 1995). The emission band close to 60 μm appears to have counterparts at $\lambda \sim 3.1\,\mu$m (Hodapp et al. 1988), whence it is clear from both this and higher resolution FIR spectroscopy (Omont et al. 1990) that the ice must take a crystalline form. Best fit models of the combined FIR and NIR spectroscopy further suggest that the ice envelopes silicate nuclei (Omont et al. 1990), and is perhaps associated with a further, smooth continuum component with optical characteristics similar to graphite (Robinson et al. 1992).

The inner lobes display isophotal contours which appear skewed, and consistent with point reflection symmetry (cf. Morris & Reipurth, 1990), a feature which may arise from internal jet activity (Roddier et al. 1995). Similar characteristics hold also for the ansae, where recent high resolution imaging has revealed the presence of narrow tails oriented in opposing directions (Langill et al. 1994). Similarly, the central bipolarity is intersected by a narrow lane of (presumably) high opacity dust, the orientation and strength of which vary critically with wavelength. Thus at visual wavelengths the central star(s) appear to be completely obscured by a band with orientation PA $\sim 72^\circ$ (Langill et al. 1994, Dougados et al. 1990). At longer wavelengths, on the other hand, the strength of the obscuration de-

creases, the PA rotates by $18.4^\circ\ \mu\mathrm{m}^{-1}$ (Langill et al. 1994), the central binary system emerges ($\lambda \sim 1.28\,\mu$m $\Rightarrow 2.1\,\mu$m (Roddier et al. 1995, Beuzit et al. 1994)), and finally the bipolarity disappears (Hodapp et al. 1988, Rouan et al. 1988); an evolutionary sequence which suggests disk optical depths $\tau \sim 1.6$ at 2.2 μm (Rouan et al. 1988), although relative central star and lobe intensities have been used to adduce values $\sim$ twice as large (Hodapp et al. 1988), and central star photometry implies $\tau \sim 0.5 \Rightarrow 1.55$ (Roddier et al. 1995).

It is apparent that the central disk also defines a region of lower polarisation (Dougados et al. 1990), is oriented at an angle $< 15^\circ$ to the line of sight (Scarrott & Scarrott 1994, Dougados et al. 1992), and may be responsible for preferential reddening of the northern lobe (e.g. Morris & Reipurth 1990). Spectroscopy of the source suggests that radial trends in grain velocity are unusual (Dougados et al. 1992), whilst modeling of polarisation (Dougados et al. 1990), infrared emission (Forveille et al. 1987), and the interior optical structure (Morris & Reipurth 1990) suggests the presence of an internal cavity of size ~ 2 arcsec, and comparatively recent cessation of mass loss (Forveille et al. 1987). Such trends may also be responsible for the absence of ionised emission in the ansae (Morris & Reipurth 1990). Adaptive optic imaging of the source at $\lambda \sim 1.28\,\mu$m, on the other hand, appears to reveal the presence of interior jets and continuing mass-loss; features which may also be responsible for generating the interior bipolar emission structure (Roddier et al. 1995; see Sect. 6)

Finally, the kinetic energy of outflow appears to be an order of magnitude larger than present central star luminosities; a disparity which may argue for a substantial decrease in luminous flux during the recent past (Forveille et al. 1987). On the other hand, it is far from clear that such trends in brightness could be easily reconciled with the expected evolution of post-AGB stars. Similarly, the overall source luminosity 200 $(D/\mathrm{kpc})^2\ L_\odot$, if supposed comparable to those of normal PN central stars ($\geq 3000 L_\odot$), would imply a distance 3.9 kpc, and height 2.6 kpc above the galactic plane; a value significantly larger than would be expected given estimated PN scale heights (e.g. Phillips 1987). It has been proposed, in consequence, that we may in reality be observing a system in the process of pre-main-sequence contraction (Langill et al. 1994, Robinson et al. 1992).

Clearly, therefore, the source is characterised by unusual, and in certain cases unique structural and kinematic properties, whilst its evolutionary status is deeply ambiguous. In the following, we present limited monochromatic imaging of the envelope in an attempt to further define the morphological characteristics of this source. We also present the results of both low and high resolution spectroscopy, with the aim of exploring spectral evolution through the outflow envelope, and determining revised velocity trends for the grain scatterers.

2. Observations

Observations of IRAS 09371+1212 were acquired using the f/15 2.54 m Isaac Newton Telescope (INT) and f/11.0 2.56 m Nordic Optical Telescope (NOT) at the Observatorio del Roque de Los Muchachos, La Palma (ORM). In the former case, an Intermediate Dispersion Spectrograph, 500 mm camera, and CCD detection element were employed, together with gratings corresponding to dispersions of 10.5 Å mm^{-1} ($\equiv 0.22$ Å pixel^{-1}; H1800V) and 66.1 Å mm^{-1} ($\equiv 1.45$ Å pixel^{-1}; R300V). As a result, we were able to obtain low resolution spectra in the blue (4240 Å $\Rightarrow$ 5070 Å) and red (6170Å $\Rightarrow$ 7010 Å), together with higher resolution observations in the red, centred upon $H\alpha$. The slit length was $180''$, slit position angle 350° (corresponding to the nebular major axis), effective spatial resolution 0.33 arcsec pixel^{-1} (although results were subsequently degraded to an effective resolution of 1 arcsec), exposure times 1000s, and seeing 0.9 arcsec. Slit widths were respectively set at 1 arcsec and 5 arcsec for the high and low resolution spectroscopy, whilst flux calibration was undertaken using the standard stars Kopff 27 at high resolution and HD 84937 at low resolution, together with an extinction curve appropriate to the ORM.

Finally, spectral calibration was undertaken through use of a Thorium-Argon lamp, together with a 2-D algorithm within the Figaro package which permits independent calibration of the differing pixel rows. Under these circumstances, the precision with which frequency can be determined depends upon the spatial/frequency sampling rate, and S/N of the relevant line; in the case of $H\alpha$ and for 1 pixel of spatial sampling, this (for the present source) is typically 0.09 Å at high resolution and 0.5 Å at low resolution. Where spatial pixels are co-added (and S/N's are correspondingly increased), errors in frequency are further reduced.

B, V, R imaging with the NOT was undertaken with the Stockholm CCD camera. Seeing was determined to be 0.6 arcsec, whilst the effective spatial resolution was approximately 0.2×0.2 arcsec^2. Unfortunately, it proved impossible to obtain an accurate calibration of our results on this particular night, and the ratio maps are therefore presented in terms of relative colour index.

3. Variations in colour index

The B/V, V/R colour maps display closely similar characteristics, and we have for this reason chosen to illustrate only a single example in Fig. 1. Casual inspection of these results reveals several interesting, and heretofore unremarked trends. In the first place, for instance, it is apparent that whilst the bright northerly interior lobe appears to display preferential reddening, as noted by several previous investigators, such properties also characterise the entire nuclear bipolar flow. Similarly, it is apparent that reduced ratios V/R extend asymmetrically into the halo, along a narrow lane extending towards the east.

Such colour asymmetries may arise in several ways. It is possible, for instance, that the interior lobes are particularly dusty, and that differences between the northern and southern components reflect comparable variations in dust outflow densities. Alternatively, and in our view more satisfactorily, it is possible that changes in the phase function $S(\alpha)$ with wavelength (see Sect. 5) result in substantial variations in scatter efficiency,

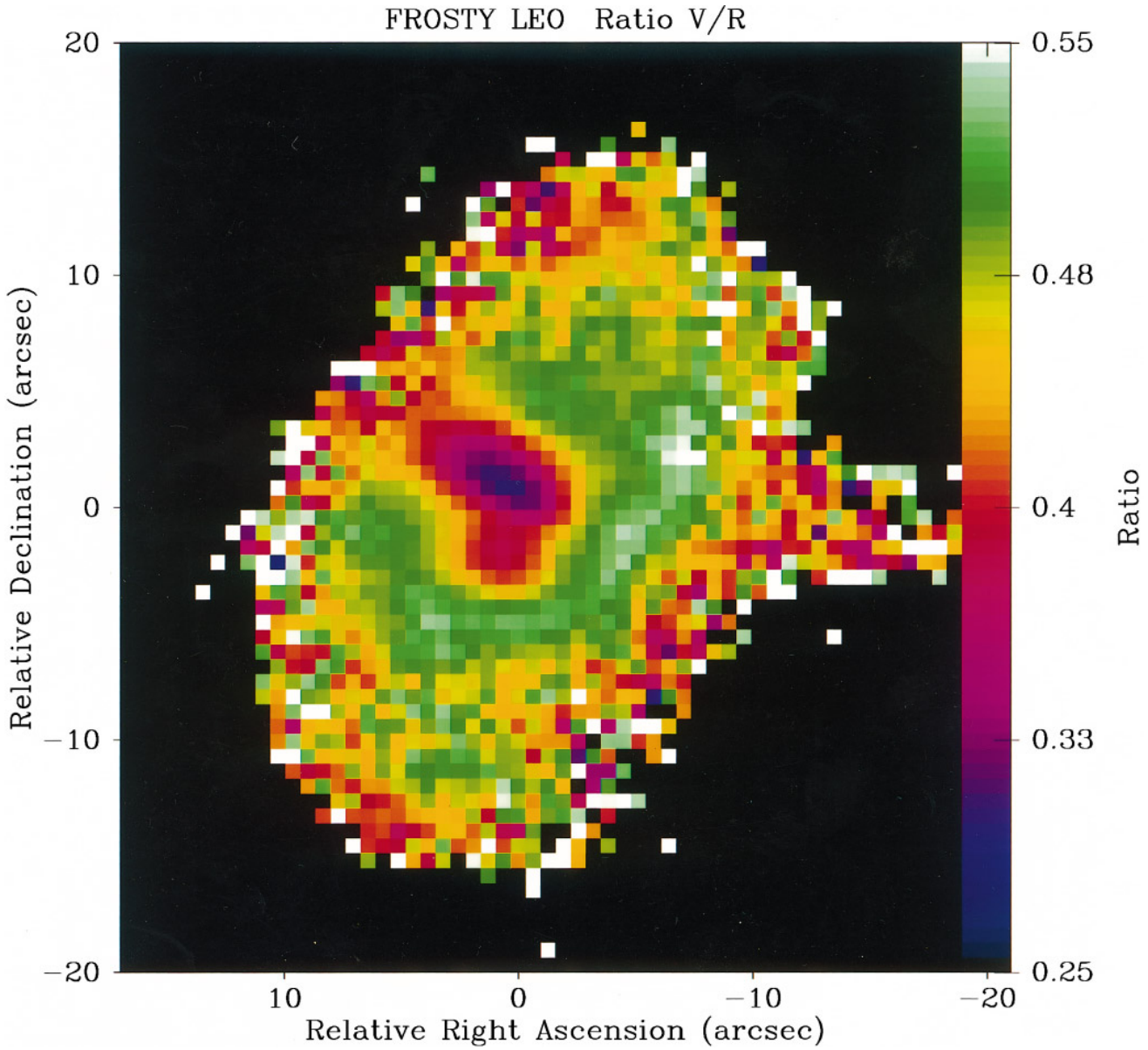

Fig. 1. V/R colour map over the envelope of IRAS 09371+1212, where we note evidence for enhanced reddening in the nucleus extending asymmetrically towards the east, and a partial annulus of reduced reddening exterior to the inner bright core. The colour coding refers to relative ratios

together with an apparent reddening of the continuum. In particular, such trends are acutely sensitive to the scattering angle, and any tilting of the flow to the line of sight would be expected to lead to scattering asymmetries between the respective lobes, and corresponding variations in spectral gradient.

Finally, it is frequently proposed that such changes in colour index arise from preferential obscuration by collimating disks – a presumption which has been liberally applied to the present source. We are considerably less sanguine that this is in fact appropriate. Noting for instance that the inclination of the disk is of order $< 15^\circ$ (see Sect. 1), and that the regime of enhanced reddening extends some 4 arcsec into the northern lobe, it is apparent that the disk radius must be of order > 15 arcsec. The disk, in brief, is required to have a structure which is both extended and thin, as noted in the conceptual diagram of Scarrott & Scarrott (1994). Such a feature would however also be expected to extend throughout the entire halo regime, resulting in appreciable distortion of colour indices along an east-west axis. We see little evidence for such trends in the current observations (Fig. 1), although it is possible that increased reddening to the east may derive from a partial disk structure.

It is interesting to note that radiation scattered from the inner halo appears to be significantly bluer than that emerging from the nucleus, although the reddening again increases towards larger radii – a trend which results in an apparent annulus of reduced reddening (Fig. 1). As for other reflection nebulae,

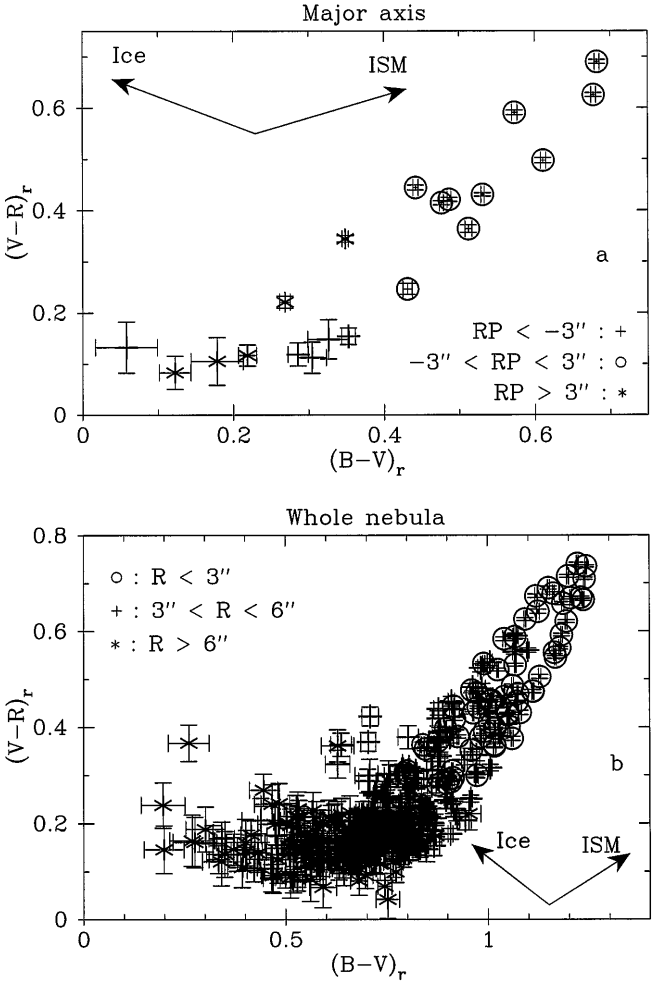

Fig. 2. Comparative variations of $(V-R)_r$ and $(B-V)_r$ for both the nebular major axis and entire nebula; note the change in gradient between low and higher values of $(V-R)_r$. Also shown for comparison are the trends expected for the interstellar medium (ISM) and model ice grains (see text for details)

we believe that such variations have a particularly straightforward explanation – the transfer of radiation to larger radii leads to reddening of the emergent radiation, and increased colour indices towards the periphery of the source. The interior reddening of the source, on the other hand, may arise from a partial belt of obscuration, or differences in grain properties between the nucleus and halo.

Some possible support for this latter hypothesis is to be noted in the relative variation of $(B-V)_r$ and $(V-R)_r$ (Fig. 2; where both here and elsewhere, the subscript r denotes relative indices). It would appear, from this, that the functional dependence between $(V-R)_r$ and $(B-V)_r$ differs as between the inner source regime (i.e. distances ≤ 3 arcsec from the nucleus) and outer halo structure; in the former case, $(B-V)_r$ decreases monotonically with decreasing $(V-R)_r$, whilst in the latter it seems that $(V-R)_r$ may actually increase as $(B-V)_r$ decreases. It is clear, in brief, that there are two distinct and disparate colour regimes, neither of which is consistent with normal reddening trends for the interstellar medium (denoted ISM in Fig. 2; the illustrated vectors are based on the work of Sapar & Kuusik (1978)), or the model ice grains of Robinson et al. (1992; model carbon grains, also considered by these authors, appear to give rise to "grey" scattering – there would be little if any change in relative $(V-R)_r$, $(B-V)_r$ indices. See also the later discussion in Sect. 5). Whether this constitutes evidence for the presence of non-ISM grains depends also however upon the level of multiple scattering, which is as yet quite ill-determined (see Sect. 5).

4. Variation of velocity through the envelope

In previous observations of the nebular spectrum by Dougados et al. (1992), line profiles over a broad swathe of wavelengths were carefully cross-correlated with the spectrum of 76 Gem (Sp. Type K5III). Systematic differences were subsequently attributed to scattering and Doppler shifting by grains within the outflow envelope. As a consequence, it proved possible to evaluate systematic trends in grain velocity over projected radial distances ~ 3 arcsec.

Velocities in the brighter southerly lobe were thereby found to be more-or-less constant, whilst for the northern lobe the trend was first for a decrease, then increase in projected velocities; the minimum velocity occurring close to the peak of the emission distribution. The sampling rate for these latter results appears to be ~ 7 times the seeing limit, however, implying that many of these velocities are not independent; the broad trend described above is consistent with a single reduced velocity at relative position -1 arcsec. Similarly, although Dougados et al. (1992) suggest the presence of substantial velocity increments to larger radii, it is clear (from their reference profile) that such trends are irretrievably compromised by instrumental scattering.

The present results, illustrated in Fig. 4, offer the possibility of a further investigation of such trends, this time using the comparatively sharp HI 6563 Å profile found in our higher resolution spectra (Fig. 3). We shall assume that the observed transition is scattered by outwardly flowing grains, and originates close to the central star – perhaps in the inner regions of a cool ionised stellar wind. Given that various investigators have suggested a termination of primary mass-loss in this source (cf. Sect. 1), this may constitute a lower mass-loss, higher velocity wind component; a pre-cursor to the stellar winds responsible for driving super-wind shells in more evolved sources (although see also our later comments). Whatever the origin, several interesting characteristics are immediately apparent:

1) As in the observations of Dougados et al. (1992), we find Doppler shifted velocities in the southern shell to be broadly invariant.

2) Velocities in the northern lobe appear to increase by $\Delta V \sim 10$ km s^{-1} out to radial distances ~ 4 arcsec, and thereafter decrease somewhat – although values at larger radial displacements are susceptible to particularly large errors because of the reduced line S/N. The velocity trends of Dougados et al. (1992),

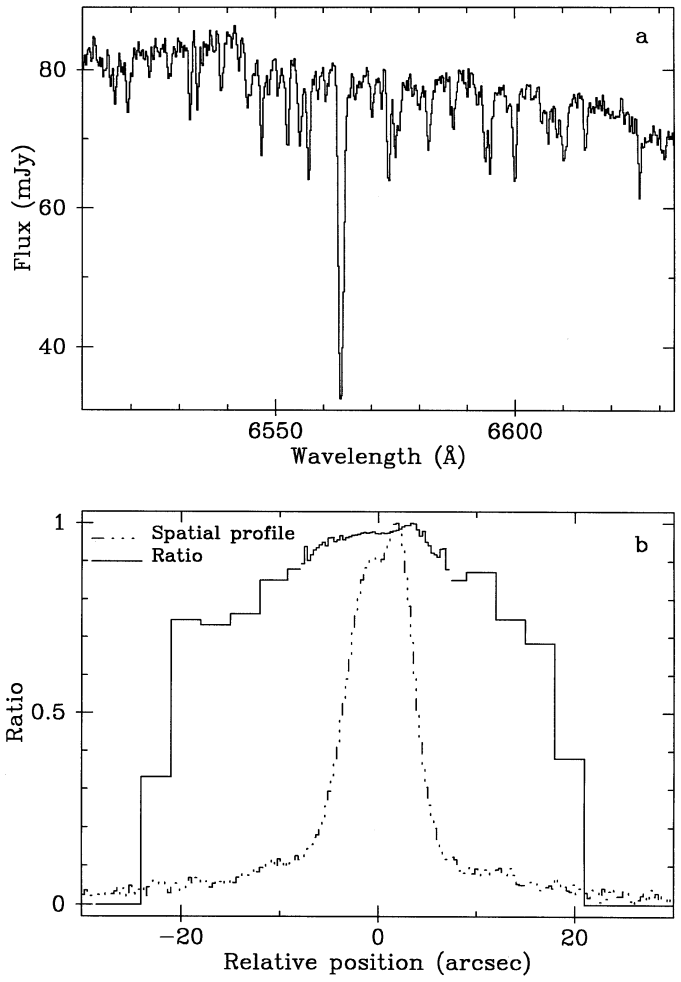

Fig. 3a and b. The $H\alpha$ absorption feature in IRAS 09371+1212 (panel a), where we have co-added all pixels along the source major axis (i.e. the spatial axis has been collapsed). Below (panel b; solid line) we also display the normalised ratio between $H\alpha$ line depth and continuum as a function of major axis displacement. The lower curve (-.-.-.-.-.-.-.) illustrates the corresponding variation in intensity at line centre

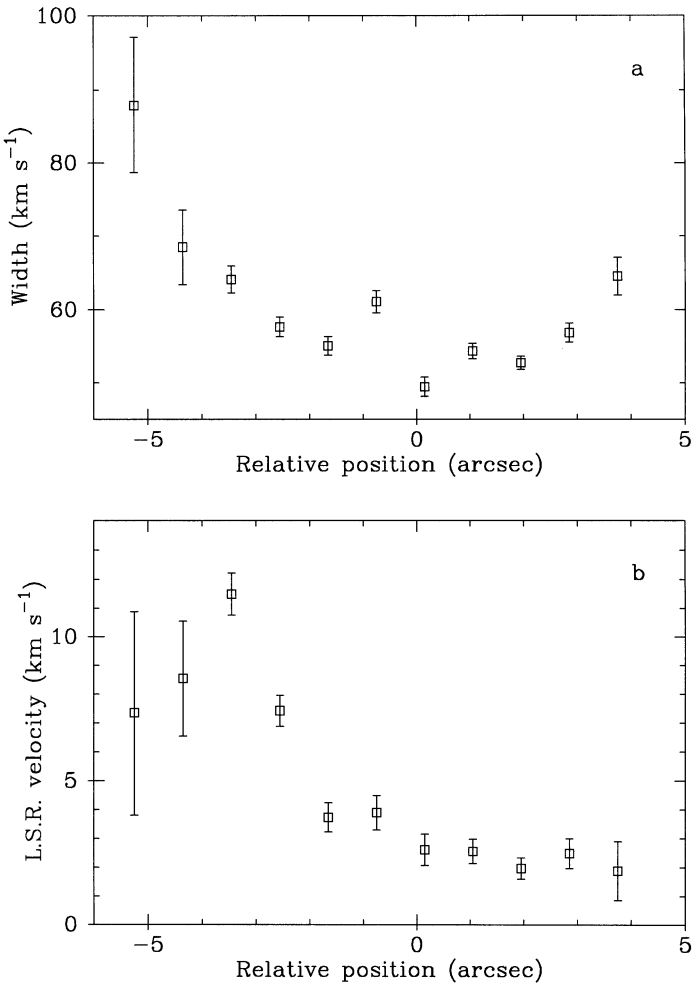

Fig. 4a and b. Variation of $H\alpha$ line width (panel a) and Doppler shifted velocities (panel b) as a function of offset along the source major axis. Note the systematic increase in both parameters for large negative radial offsets

by contrast, would lead to a distinct blip in the present results at radial offsets -1 arcsec; a deviation which is not observed.

It is of course conceivable that the difference in wavelengths between the present observations and those of Dougados et al. (1992) may also lead to a variation in scatter velocity trends; that the longer-wave observations of these latter authors may be influenced by lower grain scatter efficiencies, and reduced source optical depths. Such an effect would be unlikely, however, to explain the level of departure between their results, and those presented in Fig. 4.

3) LSR velocities are similar to (if somewhat larger than) those observed Dougados et al. (1992) (although note also the uncertainty of $\sim 4\,\mathrm{km\,s^{-1}}$ in absolute velocities implied by calibration errors). Given a central source $V_{\rm lsr} \cong -10\,\mathrm{km\,s^{-1}}$ based on the CO observations of Forveille et al. (1987), radial velocities with respect to the nucleus would be on the order of $\sim 12\,\mathrm{km\,s^{-1}}$, rising to $\sim 20\,\mathrm{km\,s^{-1}}$ at large negative axial displacements.

4) Line widths at the core take minimal values $\Delta W \sim 50$ km s^{-1}; a value which, if representative of the intrinsic width of the line source, suggests a velocity range at least comparable to that of the CO shell. For displacements towards the north and south there is a systematic, and largely symmetric increase in ΔW – although widths towards the north appear to achieve particularly large values of order ~ 90 km s^{-1}.

5) The ratio between the depth of the $H\alpha$ line and nearby regions of continuum appears also to be variant. Thus, in Fig. 3b, we see that the normalised ratio varies by a factor $\sim$ three between the exterior and interior of the source.

How are we to interpret these results? Previous studies of scattering within spherically symmetric dusty envelopes have been undertaken Dougados et al. (1992), Blerkom & Blerkom (1978), and Romanik & Leung (1981). It is apparent from this work that where multiple scattering is dominant, and the source

is spatially unresolved, then line widths will increase as a result of large grain albedos, physically thick shells, low rates of forwards scattering (i.e. smaller particles), and increased scattering optical depths; all of which effects will also tend to increase shifts in line centroid velocities by amounts comparable to the velocity of the scattering medium. Applications of such analyses to resolved outflows suggests that multiple scattering sources with broadly constant outflow velocity will, under most circumstances, result in line shifts which are also constant, and comparable to the grain expansion velocity (Romanik & Leung 1981).

It would appear, in brief, that it is extremely difficult to comprehend depressed Doppler-shifted velocities in terms of multiple scattering outflow shells. Dougados et al. (1992), by contrast, have evaluated single scattering solutions for spherically symmetric shells, finding that Doppler-shifted velocities may under these circumstances be considerably reduced. Similarly, it is found that velocity trends may be contrived which are similar to those observed here, providing that the internal cavity is sufficiently large. Such models would also, however, require that scattering grains are small (the decrease in scatter velocities is reduced where forward scattering is appreciable), and imply either line splitting towards the nebular core (which is not observed), or greatly reduced grain velocities with respect to the CO envelope (which is physically improbable). An alternative model by these authors supposes a mix of grain scattering from the collimated outflow and central disk, and would be inconsistent with the present results.

In the following, we investigate the trends expected for grain scattering within a more realistic bilobal configuration. We will show, in consequence, that depressed scatter velocities would also be anticipated where forward scattering is appreciable, and the central cavity is either small or non-existent. We also discuss various alternative models, whereby scattering occurs within cavity outflows arising from shock structures, or internal jet activity.

5. Outflow scatter models

5.1. Grain scattering model

We shall investigate scattering within the bilobal outflow configuration illustrated in Fig. 5, where the scatter regime is defined by two spherical volumes tangentially connected at the outflow source (a configuration similar to the projected structure of the interior lobes). We shall also assume that the source major axis is inclined at angle $\sim 90^\circ$ to the line of sight (in conformity with estimated disk inclination angles) and, initially, that the level of multiple scattering is low. Under these circumstances, there are at least two mechanisms whereby reduced scatter velocities may arise. In the first of these, forward scattering by grains would lead to preferential sampling of the foremost part of the shell – that is, the regime closest to the observer. Secondly, if extinction through the shell were in any way appreciable, this would again lead to preferential sampling of similar regions of the outflow. In both cases, therefore, the observer would detect sectors

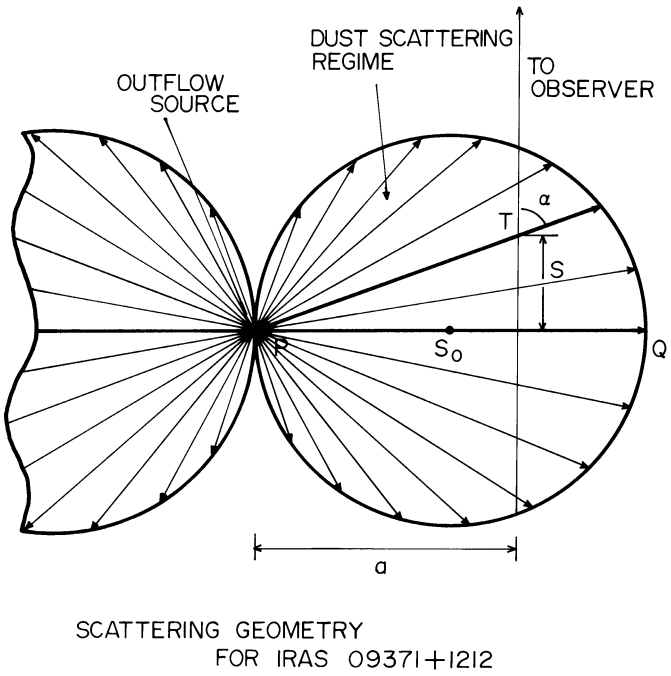

Fig. 5. Schematic grain scattering geometry for IRAS 09371+1212; the bimodal distribution is almost certainly collimated by a circumnebular disk (not shown here). Certain of our models also assume an evacuated interior zone with radius r_o

of the outflow biased towards Doppler-shifted radial velocities $V_d(1 - \cos\alpha) < V_d$ – an effect which would be accentuated were the outflow to possess internal cavities.

We can place this analysis on a more concrete footing by determining specific mean scatter velocities for the model illustrated in Fig. 5. For this case, assuming a dust outflow velocity V_d, an empirical scattering function $S(\alpha)$, and extinction optical depths τ_r between the source S and scattering element T, and τ_s between point T and the observer (i.e. along the line-of-sight scatter column), we determine a fractional radial velocity,

$$\frac{V_s}{V_d} = \left\{ \int_0^{\sqrt{1-|1-a|^2}} \frac{e^{-(\tau_r+\tau_s)}}{\left[s^2+a^2\right]^{1+\xi/2}} S(\alpha)(1-\cos\alpha)ds + \int_{-\sqrt{1-|1-a|^2}}^{0} \frac{e^{-(\tau_r+\tau_s)}}{\left[s^2+a^2\right]^{1+\xi/2}} S(\alpha)(1+\cos\alpha)ds \right\} \Bigg/ \int_{-\sqrt{1-|1-a|^2}}^{\sqrt{1-|1-a|^2}} \frac{e^{-(\tau_r+\tau_s)}}{\left[s^2+a^2\right]^{1+\xi/2}} S(\alpha)ds$$

where $S(\alpha)$ is the van Houten (1961) phase function, the radial variation in grain number density is taken to be $n_{gr} \propto r^{-\xi}$, the scatter angle is $\alpha = \tan^{-1}(a/s)$, and we employ the expressions

$$\tau_r = \tau_o \int_{r_o}^{\sqrt{s^2+a^2}} \frac{dr}{r^{2+\xi}} \Bigg/ \int_1^2 \frac{da}{a^{2+\xi}}$$

$$\tau_s \;=\; \tau_o \int_s^{\sqrt{1-|1-a|^2}} \frac{ds}{\{s^2+a^2\}^{1+\xi/2}} \Bigg/ \int_1^2 \frac{da}{a^{2+\xi}}$$

Note that spatial parameters have been normalised with respect to the lobe radius R ($\equiv 0.5a$; where a corresponds to the central ~ 3.5 arcsec bipolar core radius), and optical depths are normalised with respect to τ_o, the extinction between S_o and Q (Fig. 5). For certain simulations we have also assumed the presence of a central cavity with radius r_o.

A summary of results deriving from this model is provided in Figs. 6 and 7, whence several features are noteworthy. In the first place, and as might have been expected, the degree to which scatter velocities are depressed is a strong function of the parameters ξ, τ_o, r_o and g.

The trend of V_s/V_d with respect to impact parameter is also strongly variable, and it is apparent (for instance) that whilst interior cavities lead to an appreciable depression in V_s, such features would be unlikely to explain observed velocity trends. Similar arguments apply to outflows having strong density gradients $\xi \geq 1$ (the decline of V_s/V_d with decreasing a is steeper than observed, and similar to trends determined for forward scattering alone), and for constant density outflows, where V_s/V_d first decreases, and then again increases as a declines.

On the other hand, the contrary variations for the $\xi < 1$ and g profiles permit us to construct a tolerable simulation of observed velocity trends, providing the following conditions are satisfied:

a) The density gradient term ξ is small, and less than unity.

b) Extinction τ_o is ≥ 2.0.

c) The grain asymmetry parameter g is modest, and of order ~ 0.25.

Two characteristic series of solutions are illustrated in Fig. 7, where we have taken $\xi = 0$ for the case B profiles. In the case of the intermediate solutions A, a density function of type $n_{gr} = (x+y)^{-1/2} = fr^{-1/2}$ was found to be both analytically and numerically convenient, where $f = ((1+s^2/a^2)^{1/2}/(1+s/a))^{1/2}$. It is apparent, in both cases, that V_s/V_d is constrained to lie within a range $\sim 10\%$ of observed ratios (~ 0.5) over radial distances $a/R_o \leq 1$, and thereafter increases rapidly towards a terminal value of unity; a trend very similar to that noted in Fig. 4. The profiles determined for a modest internal cavity appear similar to those evaluated for lower values of r_o, providing somewhat smaller values of g are employed. Similarly, and as might have been anticipated from the trends illustrated in Fig. 6, the values of g required for case A are significantly less than those for case B – although the form of the profiles is again broadly similar. It is conceivable, of course, that some 'ideal' density function could be devised, strategically perched between those for $\xi = 0$ and $\xi = 1$, in which the value of g is even lower. For most realistic solutions, however, it is apparent that g must take a value which is moderately large. One further point. We find that the regime of parameter space $\xi - g - r_o$ for which these or similar solutions are available is reasonably extensive, and such variations as we deduce here should therefore be fairly characteristic for

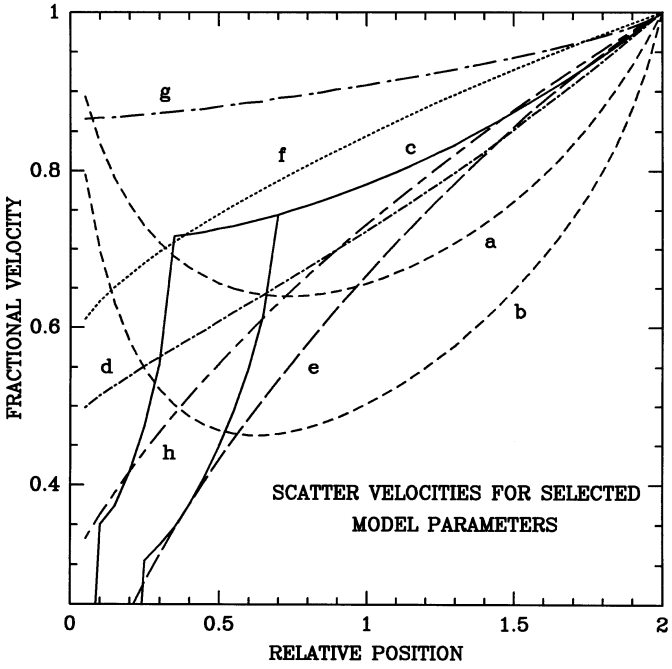

Fig. 6. Variation of fractional velocity V_s/V_d (see text) as a function of normalised distance r/R from the central star (where R is the radius of the outflow lobe (see Fig. 6)), and a variety of representative model parameters: a) $\xi = 0, r_o = 0.05, \tau_o = 2.25, g = 0.0$; b) $\xi = 0, r_o = 0.05$, $\tau_o = 5.0, g = 0.0$; c) $\xi = 0$, $r_o = 0.35, 0.7$, $\tau_o = 0.6$, $g = 0.2$; d) $\xi = 1$, $r_o = 0.05$, $\tau_o = 1.5$, $g = 0.0$; e) $\xi = 2$, $r_o = 0.05$, $\tau_o = 1.5$, $g = 0.0$; f) $\xi = 0$, $r_o = 0.05$, $\tau_o = 0.0$, $g = 0.3$; g) $\xi = 2$, $r_o = 0.05$, $\tau_o = 0.0$, $g = 0.15$; h) $\xi = 1$, $r_o = 0.05$, $\tau_o = 0.0$, $g = 0.7$. Note that ξ is the exponent of the grain radial density variation, r_o is the radius of the inner zone of evacuation, τ_o is the optical depth between S_o and Q (Fig. 6), and g is the grain scattering asymmetry parameter (see text for details)

BPN - or at least those for which the inclination is low, outflow velocities are constant, grain sizes are moderate (see below) and multiple scattering does not completely dominate.

Constraints upon ξ, τ_o, g and r_o depend also upon the adopted model geometry, and it is therefore important to note that the case illustrated in Fig. 5 is likely to represent only a broad approximation to the intrinsic source structure. In particular, it is probable that the variation of illumination/density within interior of the source departs considerably from what is assumed here. Nevertheless, the broad conclusions of this analysis are likely to apply for any more realistic modeling, and appear also to be consistent with certain other observed trends. Thus, a $\xi > 1$ variation would almost certainly lead to steeper gradients in scatter intensity than are in fact observed – excepting, of course, one adopts some extremely contrived outflow structure.

Although outflow velocities in the northern lobe may therefore be simulated reasonably adequately through the model described above, the southern lobe appears to display a distinctly differing kinematic profile (as noted earlier in Sect. 4). Such disparities may develop where there is an asymmetry of flow

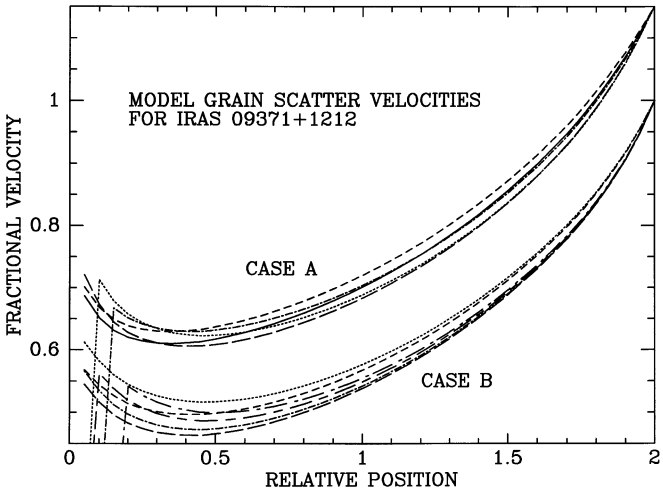

Fig. 7. Model fractional velocities V_s/V_d calculated for the case A and case B radial density variations (see text for details). Note that the fractional velocities for case A have been increased by 0.15 to avoid confusion with those for case B. The parameters for the various curves in case A, taken from top to bottom at relative position 0.8, are given by: 1) r_o = 0.05, τ_o = 2.25, g = 0.23; 2) r_o = 0.15, τ_o = 2.8, g = 0.15; 3) r_o = 0.05, τ_o = 2.5, g = 0.23; 4) r_o = 0.1, τ_o = 3.2, g = 0.075; 5) r_o = 0.05, τ_o = 3.0, g = 0.15. The corresponding parameters for case B are: 1) r_o = 0.05, τ_o = 2.5, g = 0.23; 2) r_o = 0.05, τ_o = 2.5, g = 0.27; 3) r_o = 0.2, τ_o = 3.0, g = 0.2; 4) r_o = 0.1, τ_o = 3.0, g = 0.23; 5)r_o = 0.05, τ_o = 3.0, g = 0.26; 6) r_o = 0.05, τ_o = 3.0, g = 0.28

and/or illumination, such that (say) the southerly lobe is more extensive, and R_o greater. The increase in velocity would therefore occur at larger projected distances from the nucleus, in a regime which has yet to be observed. Similarly, and for reasons cited above, it should be noted that the enhancement in V_s/V_d for $a/R_o < 0.2$ may be less than supposed here; although this regime is in any case likely to be masked by the collimating disk.

Finally, for most normal grain species (graphite, ice and so forth) the asymmetry parameter g is related to grain radius a_g through a relation of kind $a_g \cong 0.38\lambda(g{+}0.21)$, providing $0.1 < g < 0.55$, and λ is taken to be the wavelength of observation. For λ = 0.66 μm and $g \sim 0.25$ we therefore determine $a_g \sim 0.1$ μm. Such values are typical of those normally assumed for the ISM and late-type outflows; a result which suggests that grain scattering in optically thin flows will, under most circumstances, be expected to lead to a similar suppression in Doppler shifted velocities. Such grains would not however explain the similarity between scattered and (putative) central star continua noted by Mauron et al. (1989). Similarly, models of core-mantle grains by Robinson et al. (1992) suggest radii $a_g \sim 0.32$ μm, and a corresponding range $0.4 < g < 0.6$ at visual wavelengths - values substantially larger than are found to be necessary here; although the authors again assume that the IR spectrum may be simulated using spherically symmetric models.

It is clear, therefore, that a single scattering solution shows some promise in explaining the primary velocity trends within Fig. 4. On the other hand, various uncertainties must also be resolved before any such model can be fully accepted. In particular, we note that line-widths appear to increase towards the periphery of the source (Fig. 4) – a trend which would be inexplicable in terms of the single scattering solutions outlined above, but might be anticipated were multiple scattering to increase with radius. Such a presumption would also gain credence from the decrease in relative line depths noted in Fig. 3. It is conceivable, therefore, that the source possesses a range of scattering regimes, with single scattering relevant for the inner envelope ($r < 2.5$ arcsec), and multiple scattering dominant at larger radii. Such a model would in turn, however, appear to conflict with the high levels of interior polarisation noted by Scarrott & Scarrott (1994); a feature which may imply appreciable levels of multiple grain scattering at low radial offsets as well.

A further question relates to the origin of the $H\alpha$ line cores. If (as suggested earlier) these derive from an interior wind, then pre-scatter line velocities would be blue-shifted relative to the central source (an effect which has not been incorporated into the analysis above). On the other hand, it is worth noting that mean red-shifted $H\alpha$ line velocities are not appreciably different from those of the photospheric absorption lines (Dougados et al. 1992), suggesting that any such effect is likely to be small. Perhaps more critical, however, is the fact that one must presumably assume an initial regime of wind deceleration or acceleration in order to explain interior source line-widths of $\sim$ 55 km s^{-1}; a process which would normally be expected to yield strongly asymmetric line profiles. We see little evidence for such asymmetries in the present results. It is therefore possible, yet again, that multiple scattering must be invoked to explain line broadening at low radial offsets.

Finally, the high values of optical depth τ_o implied by the present analysis would require grain albedos < 0.3, and the presence of unusually absorptive scatter particles; a possibility which is by no impossible, but is, perhaps, a little unexpected.

Given such reservations and uncertainties, it is therefore of interest to investigate alternative models of grain scattering, in which the mass structure of the outflow is presumed to be considerably less uniform.

5.2. Cavity outflow models

We have heretofore assumed that scattering arises in a uniform outflow environment, wherein internal cavities are either small or non-existent. Such a prescription may not be appropriate to the present source.

In particular, bi-lobal outflows may acquire appreciable low-density cavities through one of at least two mechanisms. In the first of these, a stellar wind shock interacting with the super-wind envelope would be expected to give rise to a thin, highly compressed post-shock zone as recently described by Cuesta et al. (1995). The second possibility, adumbrated by Roddier et al. (1995), would arise where rotating jets deriving from the central binary system create a conical emission regime. In both cases, velocity vectors at some distance from the central star would be expected to be closely tangential to the nebular surface.

Such structures would also be expected to give rise to certain characteristic observational consequences. In the first place, one would anticipate evidence for a thin shell configuration in the projected emission structure, as is observed for certain other bipolar outflows such as NGC 6537 and Hb 5 – we see no evidence for such features in IRAS 09271+1212. Similarly, reflection of central star radiation from the front and rear cavity walls might be expected to result in line splitting, for which we again see little evidence in the present source.

By way of amelioration, it is possible to suppose that scattered radiation derives from one side of the cavity alone, as a result of high scattering/extinction optical depths at the front surface of the outflow, and/or flow inhomogeneities. Similarly, the broad line widths (Fig. 4) and limited S/N of the HI absorption feature would mask line splitting of order $\leq 30\,\mathrm{km\,s^{-1}}$.

How, then, might such mechanisms explain the observed velocity trends? In the case of shock interaction between wind and envelope, the similarity between the southern and northern velocities at low radial offsets may be attributed to scattering from the front surface of the outflow alone. Subsequent curvature of this surface away from the observer (viz. the discussion of Cuesta et al. (1995)) might then be expected to yield an increase in radial velocities as projected radial distances increase, such as is in fact observed; whilst appreciable curvature within finite observing apertures may also result in apparent line broadening.

The jet mechanism of Roddier et al. (1995) implies a similar, if somewhat differing formulation – although their outflow parameters require some modification in the light of present results. Thus, Roddier et al. suggest that increases in velocity to high northerly radial offsets may arise from a shift in the emission regime, whereby at low radial offsets we are observing the cavity wall located nearest to the observer, whilst for larger distances from the nucleus we are measuring the rear sector of the shell.

There is nothing a priori to object to in such an hypothesis (apart, perhaps, from a certain element of contrivance), although we note that (i) Roddier et al. use the radial velocities of Dougados et al. (1992) to determine a nebular inclination angle 74° to the line of sight – the present results would suggest a value closer to $\sim 90^\circ$; and (ii) such a mechanism would not explain the change in line widths noted in Fig. 4. One might note, in parenthesis, that the present results also militate against the presumption of Roddier et al. that it is the *northern* lobe which is tilted towards the observer.

We propose, therefore, that if this latter mechanism is indeed applicable to the present source, then the increase in radial velocity towards the periphery of the northern lobe may arise from a blending of emission from front and rear cavity walls, and that increased line widths derive from the (unresolved) contributions of these components taken together. Such a process would, at most, be expected to result in a $\sim$ doubling in line width to $W = \Delta V + \Delta W$, where ΔV is the difference in line-of-sight velocity between front and rear shells; greater widths would almost certainly lead to discernible line splitting, excepting where there is a corresponding increase in width ΔW associated with the individual cavity walls.

Taking the results cited in Sect. 4, we then determine $\Delta V \approx 40\,\mathrm{km\,s^{-1}}$.

Both mechanisms therefore appear plausible at this rather basic level of analysis, and further more detailed discussion would be of considerable interest.

6. Evolutionary status

As noted in Sect. 1, the evolutionary status of IRAS 09371+1212 is far from well established. Both Langhill et al. (1994) and Robinson et al. (1992) have noted that the height of this source above the galactic plane is extraordinarily large for a PN, unless, that is, we assume the central star to be distinctly underluminous. As a result, it has been suggested that we may be observing a star at the reverse end of the evolutionary scale, in the throes of pre-main-sequence contraction.

In assessing these various claims, it is perhaps as well to commence by drawing up an inventory of the problems and advantages associated with each hypothesis. In the first place, therefore, it may be noted that whilst bipolar outflows and jets are indeed associated with star forming centres, few if any of these possess the comparatively simple pseudo-symmetric structure which we observe in the present source. Perhaps rather more damning, however, is the fact the both the CO profile and emission strength are characteristic of extreme mass-loss AGB stars (the probable pre-cursors of PN; e.g. Knapp et al. 1989), and comparatively young bipolar PN such as CRL 618, CRL 2688, and NGC 7027 (e.g. Phillips et al. 1991, 1992), rather than the more widespread and complex pattern of emission which characterises star-forming centres. Indeed, the comparatively isolated nature of this source, with little evidence for globules, or any other of the appurtenances normally consequent upon star formation, would make this a very unusual pre-main-sequence object. Similarly, the height of the source above the galactic plane places it well outside the regimes of HI/FIR/molecular emission taken to indicate primary star-forming activity; if the source is indeed a newly formed star, then its location would appear again to be extremely anomalous.

By comparison, we believe that the case in favour of a post-main-sequence outflow is very much clearer. The observed bipolar morphology and associated ansae are well established features for important subgroups of PN – including those undergoing transition from the AGB tip through to fully fledged PN; cases possessing a close degree of morphological (and, in all probability, evolutionary) similarity include CRL 618 and 2688, whilst comparable ansae-like structures are to be found in NGC 7009 and NGC 6905 (e.g. Cuesta et al. 1993, Balick 1987). The CO profile is also (as noted above) characteristic of AGB type stars and PPN, and presumably derives from a recently ejected superwind envelope.

In supporting this identification, however, we must also tackle the serious issue of its large distance above the galactic plane, and/or underluminous central star, depending upon what distance one chooses to assume. Let us suppose first of all, therefore, that the central star luminosity is indeed comparable to that of other post-AGB stars, and that the height above the

galactic plane is 2.6 kpc or thereabouts (in fact something of an upper limit, since we have not allowed for the (uncertain) effects of extinction in determining the distance).

The statistical distribution of PN above the galactic plane is usually assumed to follow an exponential trend, although this is little more than a convenient approximation to what may, in reality, be a more complex variation; the distribution near the mid-point of the galactic plane, for instance, is rather poorly represented by such a function. Similarly, the scale height of this variation is far from adequately established, dependent as it is upon ill-determined distance scales and less-than-complete nebular samples (Phillips 1989). Taking nevertheless a scale height $k \cong 3.33$ kpc^{-1} (Pottasch 1994), and a total galactic population of PN N_t = 3 10^4 (Phillips 1989), the number of PN one would expect to observe at distances $h \geq 2.6$ kpc above the galactic plane would be of order $n_p(\geq 2.6 \text{ kpc}) = N_t \exp(-kh) \cong 5$, whilst a ten percent reduction in h would increase this total by a factor ~ 2.4.

It is clear therefore that even on a simple reading of PN spatial statistics, the chances are quite high that at least a few PN will possess large values of h; although the fact that one of this select band of sources is undergoing transition-phase evolution would continue to represent something of a surprise.

It is also possible to assume, of course, that the distance to the source is very much less than 3.9 kpc, and the height correspondingly less – bringing it, as it were, within the statistical main-stream of planetary nebulae. For this case, however, the source would be required to be distinctly underluminous compared to post-AGB evolutionary predictions. The degree to which one perceives this as a problem depends, of course, upon the strength of ones faith in the associated modeling. Given however that some such disparity exists, it is again possible to conceive of an explanation.

An unusual feature of the present source is that the inclination of the putative central disk is required to be small; in consequence of which the central star is largely obscured. Most of the radiation that we observe is therefore re-directed, either through absorption and thermal re-emission by dust and molecules, or scattering within the bipolar nebulosity. Under these circumstances, it is possible that a large fraction of the luminous flux escapes unobserved along the approximate direction of the nebular major axis; the deduced luminosity based on observed fluxes may be very much less than the intrinsic luminosity.

Such a mechanism, however, is most obviously applicable where scattering/absorption are small in directions perpendicular to the disk plane. This is not obviously the case in the present source, as we have seen in Sect. 4; the likely presence of multiple scattering testifies to quite large scattering optical depths. Nevertheless, even for this case it is possible to conceive that flow fragmentation could lead to a degree of transparency – sufficient, say, for $\sim$ half of the radiation to escape unobserved.

It is plain, therefore, that although the height of the source is likely to remain uncomfortably high, the value of h may be less than supposed from its observed galactic latitude and luminosity. Even where this is not the case, it remains far from clear that its deduced location necessarily disqualifies it as a post-main-sequence source.

7. Conclusions

We have observed IRAS 09371+1212 using both broad and narrow band filters. As a result, we note that relative colour trends $B-V/V-R$ appear to be inconsistent with both the mean IS reddening law, and the variation deduced for model grains (Robinson et al. 1992). There also appears to be a disparity in the $B-V/V-R$ reddening gradient as between the inner and outer source envelopes – a characteristic which, together with other evidence, may indicate a corresponding evolution in grain properties.

The interior lobes display particularly low values of V/R, with some evidence for asymmetric extensions in reddening towards the east. There is otherwise little evidence for the extended, slightly tilted circumnebular disk which has been presumed responsible for asymmetric reddening of the interior lobes. We propose, instead, that enhanced reddening of the northern lobe may arise from asymmetries in dust absorption within the lobes, or the combined effects of forwards grain scattering and source tilting to the line-of-sight.

The presence of a comparatively narrow $H\alpha$ absorption feature enables us to determine reliable Doppler shifted velocities along the source major axis. As a result, we find that velocities in the southern lobe are more-or-less invariant, whilst velocities in the northern lobe show a systematic rise with increasing radial displacement. There is no evidence for the decrease in velocity cited by previous investigators. Associated with these variations are a decrease in relative line depth, and increase in line width as displacement from the nucleus increases.

We suggest that such trends may arise through a combination of multiple scattering (particularly where radial offsets are large), grain extinction and forward scattering. In particular, the last cited grain properties are shown to result in a reduction in the apparent Doppler-shifted grain scatter velocity; and whilst extinction and forward scattering taken individually are only partially successful in explaining our results, a combination of the two leads to reasonable simulations of the observed trends.

In all of the models presented here, extinction through the lobes is required to be moderately large, and of order $\tau_o > 2.0$, whilst the grain asymmetry parameter g is of order 0.25. Grain sizes are likely to be a ~ 0.1 μm, and the lobe densities more-or-less constant.

Such models would, however, appear less capable of explaining variations in line-width and levels of polarisation, and it is probably necessary to invoke at least some measure of multiple scattering. Alternatively (or additionally), it is conceivable that the mass structure of this source is distinctly less uniform than assumed above, and takes the form of a thin scattering shell enveloping a lower density cavity. Such structures may develop as a result of shock interaction between an internal wind and superwind envelope, or through the action of a highly collimated precessing jet. In either case, it may again be possible to replicate observed velocity trends through a combination of tan-

gential velocity flow and, perhaps, a judicious mixture of front and rear shell scattering.

Finally, it has been noted that the high galactic latitude of the source, together with a presumed distance of ≈ 3.9 kpc, would imply an extraordinarily large distance above the galactic plane; a feature which has been used to imply that IRAS 09371+1212 may be a pre-main-sequence outflow. We suggest that such a re-classification is premature, whilst asymmetries in scattering may have led to an overestimate in source distance. There are reasonable grounds for supposing that whilst IRAS 09371+1212 may be somewhat peculiar, it is almost certainly a post-main-sequence outflow.

References

Balick B., 1987, AJ 94, 671
Beuzit J.-L., Thebault P., Perrin G., Rouan D., 1994, A& A 291, L18
Blerkom J.v., Blerkom D. v., 1978, ApJ 225, 482
Cuesta L., Phillips J.P., Mampaso A., 1993, A& A 267, 199
Cuesta L., Phillips J.P., Mampaso A., 1995, A& A 304, 475
Dougados C., Rouan D., Lacombe F., Forveille T., Tiphene D., 1990, A& A 227, 437
Dougados C., Rouan D., Lena P., 1992, A& A 253, 464
Forveille T., Morris M., Omont A., Likkel L., 1987, A& A 176, 43
Hodapp K.-W., Sellgren K., Nagata T., 1988, ApJ 326, L61
Knapp G.R., 1989, In: Torres Peimbert S. (ed.) IAU Symp. No. 131, Kluwer Academic Publishers, Dordrecht, Holland, p. 381
Langill P.P., Kwok S., Hrivnak B.J., 1994, PASP 106, 736
Mauron N., Le Borgne J. -F., Picquette M., 1989, A& A 218, 213
Morris M., Reipurth B., 1990, PASP 102, 446
Omont A., Moseley S.H., Forveille T., Glaccum W.J., Harvey P.M., Likkel L., Loewenstein R.F., Lisse C.M., 1990, ApJ 355, L27
Phillips J.P., 1987, In: Torres Peimbert S. (ed.) IAU Symp. No. 131, Kluwer Academic Publishers, Dordrecht, Holland, p. 425
Phillips J.P., Mampaso A., Williams P.G., Ukita N., 1991, A& A 247, 148
Phillips J.P., Williams P.G., Mampaso A., Ukita, N., 1992, A& A 260, 283
Pottasch S.R., 1994, Planetary Nebulae, D. Reidel Publishing Co., Dordrecht, Holland
Robinson G., Smith R.G., Hyland A.R., 1992, MNRAS 256, 437
Roddier F., Roddier C., Graves J.E., Northcott M.J., 1995, ApJ 443, 249
Romanik C.J., Leung C.M., 1981, ApJ 246, 935
Rouan D., Omont A., Lacombe F., Forveille T., 1988, A& A 189, L3
Sapar A., Kuusik I., 1978, Publ. Tartu Astrophys. Obs. 46, 71
Scarrott S.M., Scarrott R.M.J., 1994, MNRAS 268, 615
van Houten C.J., 1961, B. A. N. 16, 509